J Mol Model (2013) 19:427–438
DOI 10.1007/s00894-012-1564-3

ORIGINAL PAPER

Low-energy conformers of pamidronate and their intramolecular hydrogen bonds: a DFT and QTAIM study

Masoud Arabieh · Mohammad Hossein Karimi-Jafari · Mohammad Ghannadi-Maragheh

Received: 8 June 2012 / Accepted: 6 August 2012 / Published online: 2 September 2012

Abstract Extensive DFT and ab initio calculations were performed to characterize the conformational space of pamidronate, a typical pharmaceutical for bone diseases. Mono-, di- and tri-protic states of molecule, relevant for physiological pH range, were investigated for both canonical and zwitterionic tautomers. Semiempirical PM6 method were used for prescreening of the single bond rotamers followed by geometry optimizations at the B3LYP/6-31++G(d,p) and B3LYP/6-311++G(d,p) levels. For numerous identified low energy conformers the final electronic energies were determined at the MP2/6-311++G(2df,2p) level and corrected for thermal effects at B3LYP level. Solvation effects were also considered via the COSMO and C-PCM implicit models. Reasonable agreement was found between bond lengths and angle values in comparison with X-ray crystal structures. Relative equilibrium populations of different conformers were determined from molecular partition functions and the role of electronic, vibrational and rotational degrees of freedom on the stability of conformers were analyzed. For no level of theory is a zwitterionic structure stable in the gas-phase while solvation makes them available depending on the protonation state. Geometrically identified intramolecular hydrogen bonds were analyzed by QTAIM approach. All conformers exhibit strong inter-phosphonate hydrogen bonds and in most of them the alkyl-amine side chain is folded on the P-C-P backbone for further hydrogen bond formation.

Keywords Bisphosphonate · Conformational search · DFT · Hydrogen bond · QTAIM · Pamidronate

Electronic supplementary material The online version of this article (doi:10.1007/s00894-012-1564-3) contains supplementary material, which is available to authorized users.

M. Arabieh
Department of Chemistry, Faculty of Sciences,
Shahid Beheshti University,
Tehran, Iran

M. Arabieh · M. Ghannadi-Maragheh
Computational Chemistry Laboratory, NSTRI,
Tehran, Iran

M. H. Karimi-Jafari (✉)
Department of Bioinformatics, Institute of Biochemistry and Biophysics, University of Tehran,
Tehran, Iran
e-mail: mhkarimijafari@ut.ac.ir

Introduction

Bisphosphonates are analogues of the naturally occurring inorganic pyrophosphate in which the oxygen in P-O-P has been replaced by a carbon, resulting in a metabolically stable P-C-P structure [1, 2]. These drugs represent a large contribution to the global pharmaceutical market and are widely used in treatment of a variety of bone disease such as osteoporosis, Paget's disease and hypercalcemia due to malignancy [3, 4]. Replacement of the oxygen atom between two phosphonic acid moieties of pyrophosphate by a carbon atom opened up the possibility of attaching side chains (1 and 2 in Fig. 1a). Over many years, a large amount of experimental research on bisphosphonates has been focused on the modulation of the characteristic features of these compounds by variation of the structure and functionality of side chains of the P-C-P backbone [5]. In the most potent bisphosphonates in clinical use, one of the side chains is a hydroxyl group and the other is a bulky group with a nitrogen moiety either in an alkyl chain or within a heterocyclic structure. These nitrogen containing bisphosphonates inhibit the enzyme farnesyl diphosphate synthase (FPPS) by binding to its active site via participation of a cluster consisting of 3 Mg^{+2} ions, as demonstrated by X-ray diffraction studies [6–9].

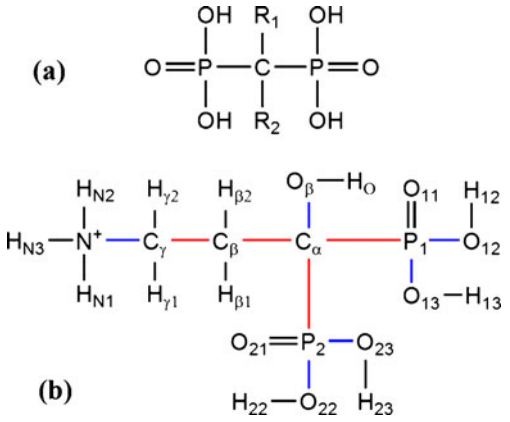

Fig. 1 **a** General structure of geminal bisphosphonates. **b** Structure of pamidronate in its fully protonated form (H_5L)

Each of the phosphonate groups, hydroxyl moiety and positive nitrogen center play a distinct role in overall activity of clinically relevant bisphosphonates, as revealed from experimental and QSAR studies [10–14]. When targeting bone mineral or FPPS enzyme each of these functional groups interact specifically with their molecular targets. For example removal or replacement of a phosphonate with other groups leads to a huge loss of activity. The length of bulky side chain and the location of its positive nitrogen center relative to the P-C-P backbone is another important parameter. The hydroxyl moiety acts also as a "bone hook" and existence of it is essential for efficient bone resorption activities. Although many experimental studies shed some light on the structure-activity relationships of bisphosphonates, it is still an open theoretical question of how small structural modifications of bisphosphonates may lead to extensive alterations in their physicochemical, biological and toxicological characteristics.

A few theoretical studies have also been conducted on bisphosphonates and their interaction with biological targets [15–18]. In 1994 Rasanen and coworkers [15] have studied the gas-phase molecular properties of two clodronate-type bisphosphonates at the HF/3-21 G* level of theory. A self-consistent reaction field (SCRF) model has been used in their work to incorporate solvent effects. They also investigated the geometry of complexes of bisphosphonates with up to six water molecules. The same authors in another work [16] have used the same methodology to investigate the interaction of bisphosphonates with cationic magnesium and calcium ions. In 2006 Robinson and coworkers [17] used the generalized AMBER force field (GAFF) to model the structure of bisphosphonates and their interaction with hydroxyapatite (a model for bone mineral). Reasonable agreement was found between vacuum molecular mechanical geometries and solid state crystal structures. They have analyzed the relative bone affinity of different bisphosphonates by comparison of the magnitude of the exothermic interaction energy released through binding to different faces of hydroxyapatite crystal. Finally, in a recent study the energetic basis of molecular recognition between FPPS enzyme and nitrogen containing bisphosphonates have been studied by Ohno and coworkers [18] using the fragment molecular orbital (FMO) method. They have found that the potency of nitrogen containing bisphosphonates is affected by hydrogen bond, electrostatic interaction, CH-π and π-π interactions with FPPS residues.

Pamidronate (Fig. 1b) is a second generation bisphosphonate which was the starting point for extensive structural modifications. Though more potent bisphosphonates have been obtained from these modifications, this compound is still a classical target for general structural investigations on a hydroxy-bisphosphonate moiety with an aliphatic alkylamine side chain. Assessment of the conformational flexibility of pamidronate and patterns of H-bonding that governs it would be helpful for analysis of interaction of this ligand and other nitrogen containing bisphosphonates with their biological targets. Moreover, knowledge of conformational states of pamidronate is a perquisite for study of its interaction and complexation with relevant metallic cations such as Mg^{+2}, Ca^{+2} and radio-nucleotides such as Sm^{+3} [19, 20]. In this regard a detailed structural analysis of bisphosphonates under a well-defined theoretical framework is necessary for prediction of their activities. In the present study, an extensive conformational search was performed to identify the most stable structures of pamidronate, as a representative member of nitrogen containing bisphosphonates pharmaceuticals. Some structural features and patterns of intramolecular hydrogen bonds over the conformational space of pamidronate will be analyzed in the following sections.

Methodology

Structural definitions

Pamidronate is a polyprotic acid having four ionizable P-OH groups and one amino ($-NH_2$) group which might be protonated in the form of a positive acidic moiety ($-NH_3^+$) (see Fig. 1b). Successive deprotonation of this pentaprotic acid (referred to as **H_5L**) results in other protonation states of pamidronate. The present study is simplified by focusing attention on those states that are more relevant in the physiological range of pH. Measured values of pK_{a1}, pK_{a2} and pK_{a5} are around 1.24, 1.93 and 12.14, respectively corresponding to the first, second and fourth ionizations of the four P-OH groups [21, 22]. Thus only the **H_3L**, **H_2L** and **HL** species at both of the canonical (c) and zwitterionic (z) forms are considered here. Note that the total charge of species is dropped in our notation.

Structure of fully protonated **H_5L** form of pamidronate is illustrated in Fig. 1b with unique atom-names that were used to facilitate the structural analysis of the system. Some useful conventions were adopted in naming of atoms in other protonation states. In the case of un-equivalent phosphonate groups, the name P_2 was always used for the P atom in that phosphonate group which has less proton than the other. Moreover, within a phosphonate or amine group protons are named in increasing order of their acidity. Thus H_{x3} (x = N, 1, 2) refers to the most acidic proton in a functional group.

As illustrated in Fig. 1b, conformational flexibility of **H_5L** is controlled by ten rotamers in its structure. Successive deprotonation reduces the dimension of conformational space to 9, 8, 8, 7, 7 and 6 in the case of **H_3L(c)**, **H_3L(z)**, **H_2L(c)**, **H_2L(z)**, **HL(c)** and **HL(z)**, respectively. Common to all species, there are four rotamers that define the heavy-atom (non-hydrogen back-bone) structure of pamidronate (red bonds in Fig. 1b). By definition, rotations of PO_3 groups are expressed in terms of X-P_1-C_α-Y (Φ_{1XY}) and X-P_2-C_α-Y (Φ_{2XY}) torsion angles where X and Y might be one of the possible proximal and distal atoms. Rotations along the alkyl-amine side-chain are expressed by C_γ-C_β-C_α-O_β ($\Phi_{\alpha\beta}$) and N-C_γ-C_β-C_α ($\Phi_{\beta\gamma}$) torsion angles. To provide compact notations for different conformations, torsion angles Φ_1 and Φ_2 are defined in a unique manner as an average over Φ_{1XY} and Φ_{2XY} values for some combinations of X and Y. Structural definitions adopted in present study were chosen to be generally applicable to other bisphosphonates in order to be helpful for future comparisons.

Following IUPAC notation for torsion angle [23], each of the above mentioned dihedrals are designated by symbols **T**, **C**, **G^+**, **G^-**, **A^+**, and **A^-** to represent trans, cis, gauche-clockwise, gauch-counterclockwise, anticlinal-clockwise and anticlinal-counterclockwise, respectively. A combination of these symbols for a set of (Φ_1, Φ_2, $\Phi_{\alpha\beta}$, $\Phi_{\beta\gamma}$) rotamers was used to identify different heavy-atom structures preceded by a number to sort, in order of increasing energy, all investigated conformers. It should be noted that for Φ_1 and Φ_2 angles, due to their average definition, only **C** and **G** (without + or −) symbols were used to reflect the eclipsed or staggered orientations of PO_3 groups around P-C bonds. Thus, for example, the **GGTT** refers to a structure in which both PO_3 groups are staggered and the whole side-chain is transoid.

Conformational search

To explore conformational space of pamidronate, a systematic variation of all rotational degrees of freedom was performed for which Φ_{1XY}, Φ_{2XY}, $\Phi_{\alpha\beta}$ and $\Phi_{\beta\gamma}$ were varied by four, four, five and five-fold increments, respectively. In the case of hydrogen-contained dihedrals (blue bonds in Fig. 1b) a four-fold incremental variation was used except for **H_3L(c)**, **H_3L(z)** and **H_2L(c)** where a 3-fold H-X-Y-Z dihedral was considered to avoid combinatorial explosion of a number of trial structures. Accordingly, 97,200, 32,400, 25,600 and 6400 structures were constructed for cases with nine, eight, seven and six rotamers, respectively.

All bond lengths and bond angles are set initially to the equilibrium values obtained from a model-builded structure that was optimized by PM6 semiempirical method. PM6 is the most recent member of the NDDO family of semiempirical methods and is understandably the most accurate [24]. Several low energy phenomena are predicted more accurately by PM6, with the most important of them being the prediction of the energies and geometries involved in hydrogen-bonding. Thus the initial structures were then partially optimized by PM6 method while all bond lengths kept frozen. This constraint helps avoid bond breaking and forming when there are bad contacts in the initial structures. The resulting structures were then fully optimized by relaxing bond lengths. To avoid loss of any minima near the initial structures, starting values of the trust radius in the following adopted eigen-vector algorithm was reduced by an order of magnitude.

Redundant conformers were identified by checking the final heats of formation and also by comparison of root mean squared atomic distances between structures. After relaxation of bond lengths it was found that the zwitter ionic forms are unstable in gas-phase and one of the protons on the NH_3^+ group tends to migrate to the phosphonate groups. To trap the zwitterionic states, solvation should be considered to stabilize charge separation by environmental effects. Accordingly, the conductor-like screening model (COSMO) was used in conjugation with PM6 Hamiltonian for optimization of zwitter ionic trial structures. COSMO is a computationally efficient continuum approach for modeling solvent effects which generates a conducting polygonal surface around the system at the Van der Waals distance [25]. In COSMO calculations 162 surface segments per atom was used with a dielectric constant of 78.4 for solvent. However, as will be discussed later, in the case of HL protonation state the canonical tautomer was preferred over the zwitter ionic one in both gas-phase and solvated structures.

Semiempirically located minimum structures were then subjected to further optimizations at the B3LYP/6-31+G* level of theory. Solvent effects were incorporated through the conductor polarized continuum model (C-PCM) [26, 27]. In the course of geometry optimizations only the electrostatic contribution to the solvation energy was considered via the iterative solver method while for the final structures the cavitation and dispersion-repulsion parts of solvation energy were also calculated at the HF/6-31+G* level. At the B3LYP/6-31+G* level, number of unique conformations was reduced

to 65, 58 and 37 for **H_3L(c)**, **H_2L(c)** and **HL(c)** respectively and the C-PCM calculations resulted in 62, 75 and 45 conformers for **H_3L(z)**, **H_2L(c/z)** and **HL(c)**, respectively. To increase the accuracy of geometries, low-energy conformers obtained at the B3LYP/6-31+G* level were further optimized at the B3LYP/6-311++G(d,p) level of theory. The normal mode analysis was also performed at this level for final structures to ensure their minimum character. The zero-point energy (ZPE) corrections and thermal contributions to the energy and entropy were also obtained from this analysis. To increase the accuracy of relative conformational energies, single-point calculations were performed on the final structures at the MP2/6-311++G(2df,dp) level with and without C-PCM model.

Conformational populations

As will be seen in the next section, many low energy conformers are possible, in gas-phase or solution, for each protonation state of pamidronate. To determine equilibrium population of these structures, standard techniques of statistical mechanics were used [28, 29]. For a given protonation state, the structure with lowest value of ZPE-corrected electronic energy was selected as reference conformer C_{ref} and the following conformational equilibrium:

$$C_{ref} \Leftrightarrow C_i \quad K_i = \frac{[C_i]}{[C_{ref}]} \tag{1}$$

was considered between the reference conformer and any of the others. The equilibrium constant K_i was obtained from molecular partition function q_i according to the following relation:

$$K_i = \frac{q_i}{q_{ref}} = K_i^{rot} K_i^{vib} K_i^{elec} = \frac{q_i^{rot}}{q_{ref}^{rot}} \frac{q_i^{vib}}{q_{ref}^{vib}} \frac{q_i^{elec}}{q_{ref}^{elec}}. \tag{2}$$

In this equation the equilibrium constant is factorized to the rotational (K^{rot}), vibrational (K^{vib}) and electronic (K^{elec}) contributions and q^{rot},q^{vib} and q^{elec} are rotational, vibrational and electronic parts of molecular partition function, respectively. For each conformer these partition functions were calculated from respective ab initio data including moments of inertia, vibrational frequencies and ZPE-corrected electronic energies. The fraction (X_i) of each conformer in the equilibrated sample was then obtained according to the following relation:

$$X_i = K_i / \sum_i K_i, \tag{3}$$

where the sum in the denominator goes through all conformers including the reference one (note that K_{ref}=1). The factorization that was adopted in Eq. 2 makes it possible to analyze in a distinct manner the role of rotational, vibrational and electronic degrees of freedom on the population of each conformer.

Characterization of hydrogen bonds

There are numerous sites in the structure of pamidronate that can potentially act as donors and/or acceptors of protons. As a result of this fact hydrogen bonding plays an important role in structural diversity of pamidronate and the relative stability of its conformers. In the present study hydrogen bonds in different conformers were identified between hydrogen and acceptor if their distances are larger than the sum of their Van der Waals radii and simultaneously if the donor-hydrogen-acceptor angle is larger than 110º. In this regard, Van der Waals radii as tabulated by Bondi were used for all atoms [30]. As an independent measure, topology of the electron density was analyzed according to the quantum theory of atoms in molecules (QTAIM) [31]. Existence of a bond critical point (bcp) between hydrogen and acceptor atoms were used as a topological confirmation of geometrically identified hydrogen bonds [31, 32]. Moreover, the value of electron density (ρ_{bcp}) and its Laplacian function $\nabla^2_{\rho_{bcp}}$ were calculated at hydrogen bonding critical points for further characterization of hydrogen bonds.

Estimation of hydrogen bond energy (E_{HB}) would be helpful for analysis of the role of hydrogen bonding on different conformers. In the case of intramolecular hydrogen bonds there is not a unique proposal for calculation of E_{HB}. In this work the relation $E_{HB}\approx 0.5V_{bcp}$ were used where V_{bcp} is the local potential energy density at the hydrogen-bond critical point [32]. This relation has been proposed from a correlation between V_{bcp} and E_{HB} over a sample of crystal structures [33]. The terms “topological measure” and “topological confirmation” in previous sentences should be used with some cautions outside the QTAIM paradigm. Despite popularity in the application of topological criteria for identification of hydrogen bonds, it should be noted that the existence of a bond critical point does not always indicate an interaction and the magnitude of the density at this point in noncovalent interactions does not always correspond to hydrogen bond strength. In the case of intramolecular interactions, which are difficult to quantify, this approach can be at least suggestive of the bond strengths.

All semiempirical calculations were performed by MOPAC [34] while DFT and MP2 results were obtained by GAMESS suite of programs [35]. The AIM2000 package [36] was utilized for QTAIM analysis of the wave function.

Results and discussions

Some of the most stable gas-phase structures of pamidronate are displayed in Figs. 2 and 3. Corresponding solvated

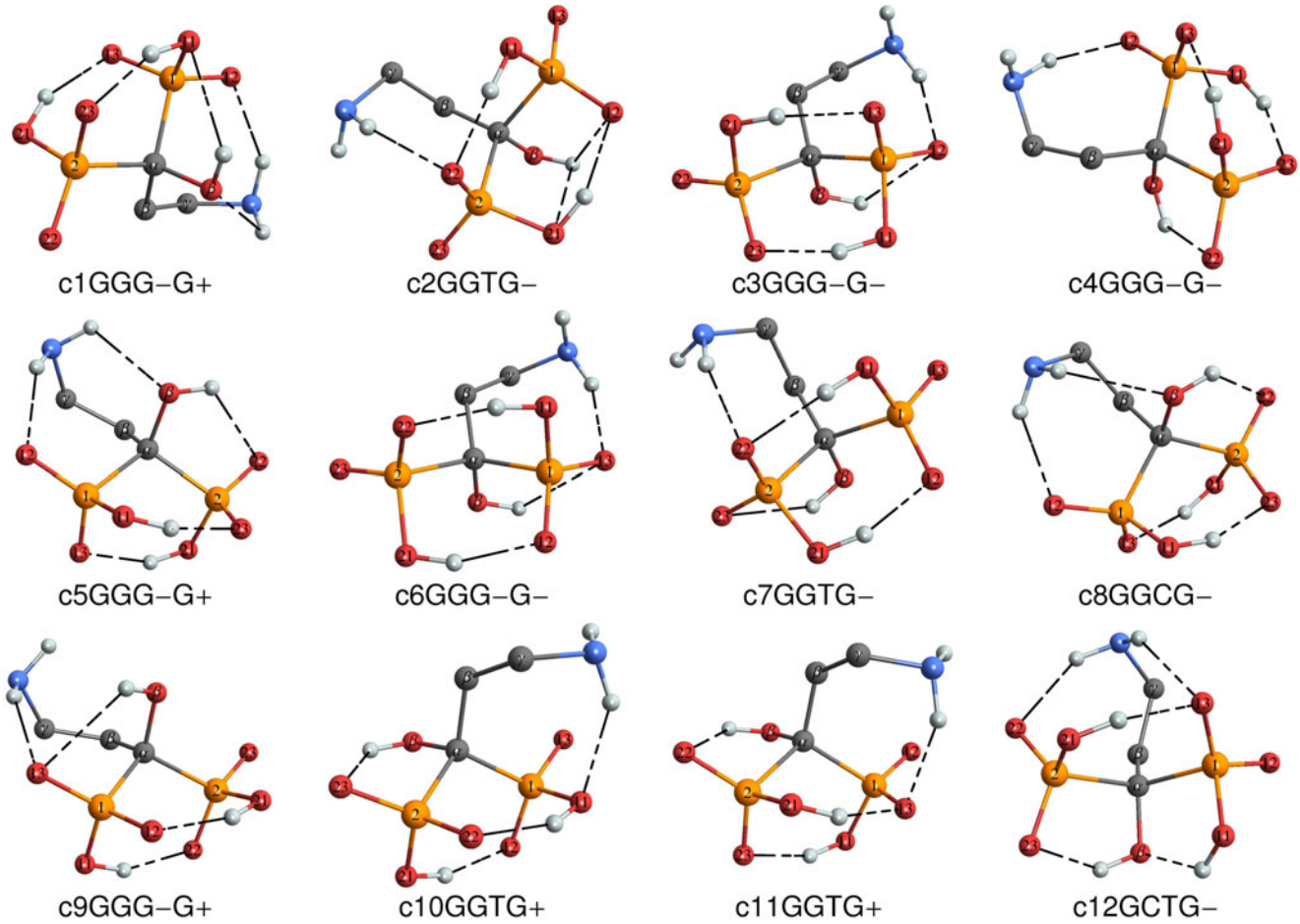

Fig. 2 Geometries of the most stable gas-phase conformers of H_2L protonation state of pamidronate

structures obtained from C-PCM calculations are depicted in Fig. 4. (Structures of all obtained conformers can be found in Figs. S1, S2. S3, S4, S5 and S6 in supplementary information). Relative electronic energies, ZPE corrected energies, Gibbs free energies, conformational populations and conformational equilibrium constants for most populated gas-phase and solvated conformers are reported in Tables 1 and 2. These data for all obtained conformers can be found in Tables S1, S2, S3, S4, S5 and S6 in supplementary information). In Table 3 some structural parameters of pamidronate for the most stable conformers obtained at the B3LYP/6-311++G(d,p) level of theory are compared with those obtained from X-ray crystallography [37, 38]. The overall agreement is reasonable considering the fact that all X-ray structures have no intramolecular hydrogen bond and have an extended conformation while all theoretical structures have a strong intramolecular hydrogen bond with folded side chain. Moreover, in X-ray structures some positively charged counter ions located near the phosphonate groups considerably affect their geometries. Wild changes in some reported angle values of theoretical conformers could be attributed to different patterns of intramolecular interactions as will be discussed in the following sections.

Canonical vs. zwitterionic stability

As noted previously, all stable gas-phase structures are of canonical form and solvation is necessary to stabilize charge-separated zwitterionic structures. However, even in the presence of continuum solvation model successive deprotonation of pamidronate destabilizes the zwitterionic forms. In the case of **H_3L**, all of the most stable conformers are zwitterion but there is a close competition between **H_2L (c)** and **H_2L(z)** conformers as is evident from relative energies and populations in Tables 2 and S4. The **z1GGTG$^-$** conformer has lowest electronic energy and ZPE-corrected energy but thermal corrections make two canonical conformers **c6CGG$^-$A$^-$** and **c2GGG$^-$G$^-$** more populated as a result of lower Gibbs free energies. Entropic and thermal effects play a significant role on the relative stability of

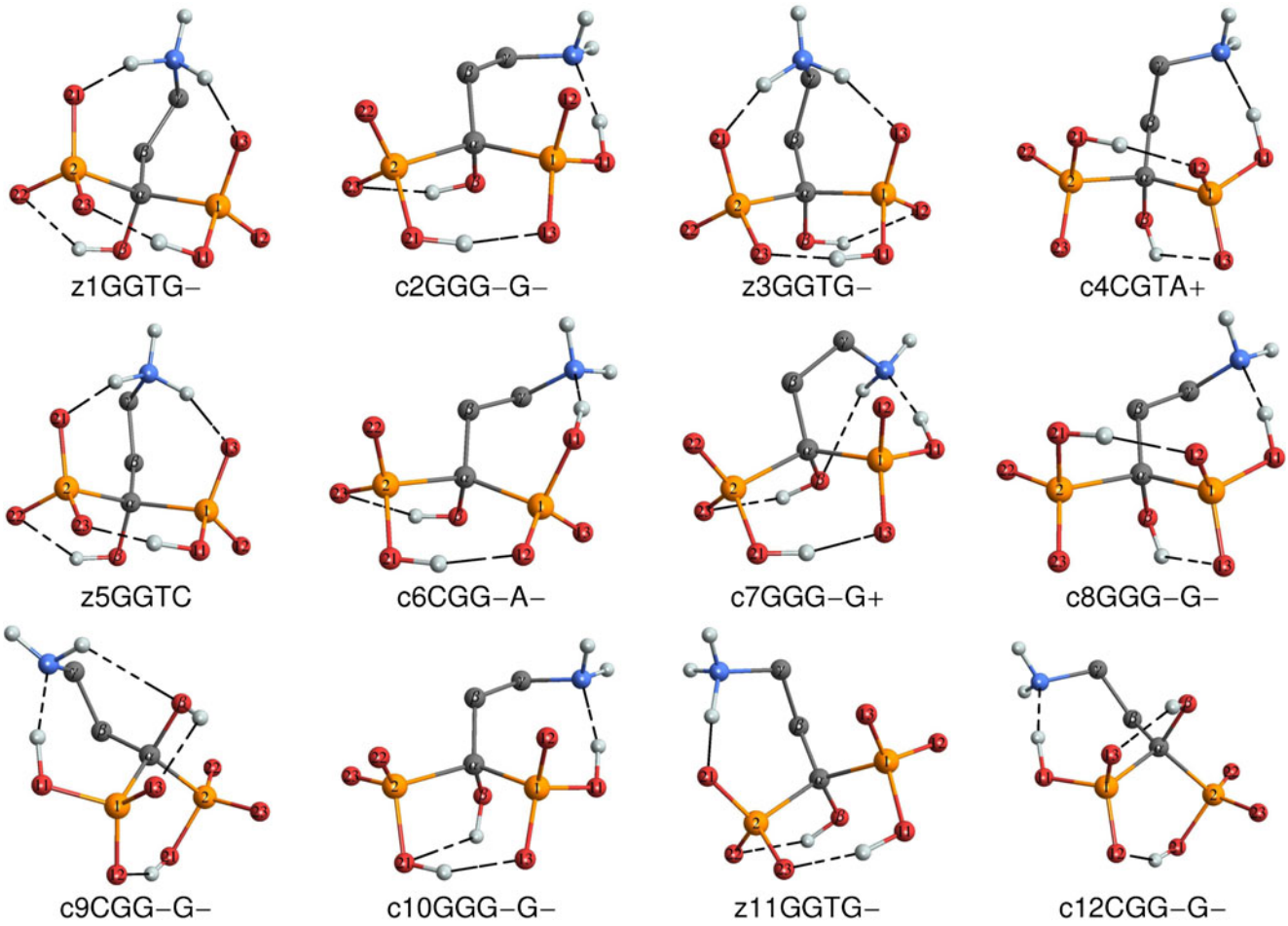

Fig. 3 Geometries of the most stable solvated conformers of H_2L protonation state of pamidronate

solvated structures in all protonation states. In the case of **H_2L** solvated structures, three of the five conformers with lowest energy are zwitterionic but after inclusion of thermal effects the total population of z-forms is less than 30 %. In the case of **HL** protonation state all solvated conformers are canonical since the phosphonate groups are highly charged and more separation of charges is impractical from the electrostatic point of view. Present calculations show that the **H_3L** form of pamidronate is mainly populated by a single conformer but the **H_2L** and **HL** protonation states are multi conformer systems in gas-phase and solution.

Electronic vs. vibrational stability

In all protonation states the differences in electronic energy of conformers are small and thus ZPE and thermal corrections have significant effect on the energy ordering of different conformers. This effect is more pronounced for solvated structures as a result of smaller successive energy differences. In this regard an interesting question would be the role of vibrational and rotational components of molecular energy on the relative stability of different conformers. There are many cases in Tables 1 and 2 and S1, S2, S3, S4, S5 and S6 for which a conformer with higher electronic energy becomes more populated than a conformer with lower electronic energy. A neat example is solvated **H_3L** conformer **z2GGTG$^-$** which is around 10 % more populated than global minimum **z1GGG$^-$G$^-$** since its K_{vib} value is larger than that of **z1GGG$^-$G$^-$**. In other words, as a result of its larger vibrational partition function, **z2GGTG$^-$** has a less rigid structure than **z1GGG$^-$G$^-$** and is more favored with respect to vibrational degrees of freedom. It should be noted that these two conformers have nearly the same K_{rot} value and with respect to rotational degrees of freedom none of these structures is preferred over the other. In other words structure of **z2GGTG$^-$** is nearly as compact as that of **z1GGG$^-$G$^-$**.

Similar comparisons can be made between electronic, vibrational and rotational equilibrium constants of other conformers in different protonation states. As a general conclusion, it can be said that relative stability of different

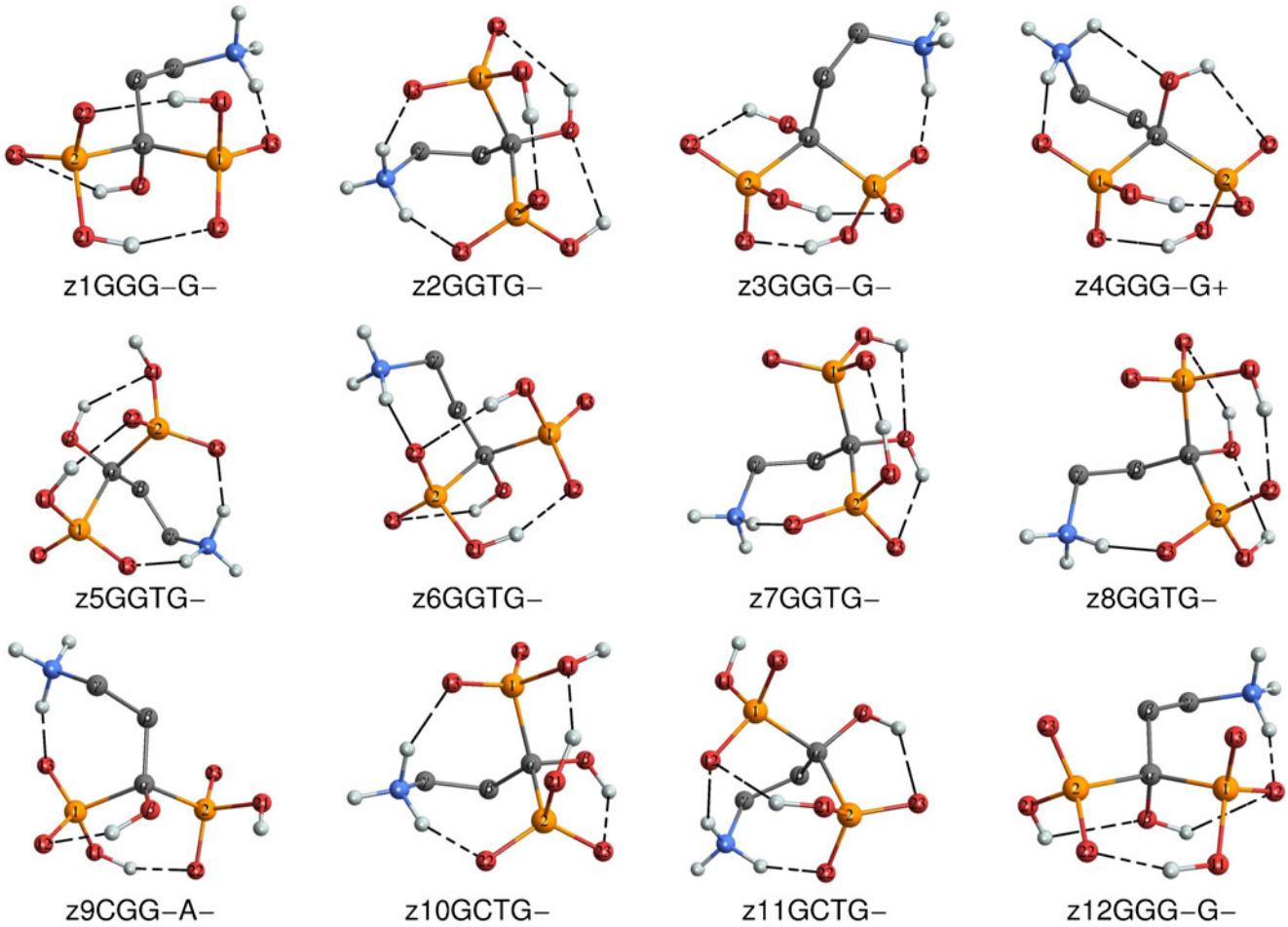

Fig. 4 Geometries of the most stable solvated conformers of H_3L protonation state of pamidronate

conformers of pamidronate in different protonation states is mostly controlled by electronic (mainly energetic) and vibrational (mainly entropic) factors. The overall effect of rotational factors is small since there are multiple hydrogen bonds in the structure of most (low-lying) conformers. Presence of these hydrogen bonds keeps most conformers in locked forms with the same level of compactness. In all conformers of **H_3L** and **H_2L** the alkyl amine side chain is folded

Table 1 Relative electronic energies (E), ZPE-corrected energies (E_0), Gibbs free energies (G), conformational equilibrium constants (K) and conformational populations of the most stable gas-phase conformers of pamidronate. Only conformers with population more than 5 % are listed here. All energies are in kcalmol^{-1}

Conformer	Population (%)	E	E_0	G	K	K_{elec}	K_{vib}	K_{rot}
H_3L								
c1GGTG-	88.5	0	0	0	1	1	1	1
c2GGG-G-	5.6	1.858	1.732	1.377	0.064	0.043	1.349	1.090
H_2L								
c1GGG-G+	43.2	0	0	0	1	1	1	1
c2GGTG-	23.7	0.181	0.543	1.08	0.549	0.737	0.780	0.955
c3GGG-G-	20.4	0.645	0.592	0.339	0.472	0.337	1.389	1.009
c4GGG-G-	7.7	1.134	1.029	0.814	0.178	0.148	1.195	1.009
HL								
c1GCG+G+	28.8	0	0	0	1	1	1	1
c2GCTG-	31.7	0.182	−0.061	−0.542	1.098	0.736	1.583	0.943
c3GCG-G+	12.9	0.523	0.324	0.077	0.448	0.414	1.078	1.005
c4GCG-G-	25.4	0.625	0.173	−0.830	0.881	0.348	2.488	1.017

Table 2 Relative electronic energies (E), ZPE-corrected energies (E_0), Gibbs free energies (G), conformational equilibrium constants (K) and conformational populations of the most stable solvated conformers of pamidronate. Only conformers with population more than 5 % are listed here. All energies are in kcal mol^{-1}

Conformer	Population (%)	E	E_0	G	K	K_{elec}	K_{vib}	K_{rot}
H_3L								
z1GGG$^-$G$^-$	36.2	0	0	0	1	1	1	1
z2GGTG$^-$	47.3	0.098	−1.115	−2.585	1.307	0.848	1.614	0.955
z3GGG$^-$G$^-$	11.0	0.232	0.960	2.162	0.304	0.676	0.448	1.004
H_2L								
z1GGTG$^-$	65.8	0	0	0	1	1	1	1
c2GGG$^-$G$^-$	15.2	1.763	0.807	−1.045	0.231	0.051	4.154	1.092
c4CGTA$^+$	5.4	2.214	1.432	−0.084	0.082	0.024	3.270	1.056
c6CGG$^-$A$^-$	5.6	2.651	1.170	−1.501	0.085	0.011	6.774	1.099
HL								
c1GCG$^-$G$^+$	14.9	0	0	0	1	1	1	1
c2GCG$^-$T	30.0	0.081	−0.183	−0.942	2.012	0.872	2.072	1.114
c3GCG$^-$T	11.1	0.177	0.363	0.546	0.748	0.742	0.902	1.117
c4GCG$^+$T	15.7	0.231	−0.549	−1.589	1.052	0.677	1.397	1.111
c5GCG$^+$T	16.0	0.424	−0.399	−1.687	1.073	0.489	1.972	1.113

on the P-C-P back bone to form one or two hydrogen bonds. Even when the alkyl amine side chain is extended and forms no hydrogen bond, as in some conformers of **HL**, the rotational partition function does not change considerably and electronic and vibrational factors remain more effective.

Other notable cases of competitive role of electronic and vibrational factors occurs in gas-phase **HL** conformers where **c2GCTG$^-$** and **c4GCG$^-$G$^-$** are more populated than **c1GCG$^+$G$^+$** and **c3GCG$^-$G$^+$**, respectively. The same thing is true for solvated conformers of **HL** where **c2GCG$^-$T** is considerably more favored over **c1GCG$^-$G$^+$** and both of **c4GCG$^+$T** and **c5GCG$^+$T** conformers are more preferred than **c3GCG$^-$T.**

Statistical analysis of P−O bond lengths

Two histograms of P−O bond lengths with equal bin widths of 0.008 Å are depicted in Fig. 5 for gas-phase and solvated conformers. Continuous or dashed curves in this figure were obtained from a smooth Gaussian kernel representation of the distribution of whole or some special subsets of P−O bond length data. As can be seen, values of P−O bond length are clustered into two distinguishable distance ranges depending on the protonation of oxygen atom. Single P−O bonds (blue curves in Fig. 1b) are obviously longer and cover a range from 1.58 to 1.75 Å in gas-phase conformers. This range is contracted considerably in the solvated conformers and as a rule

Table 3 Some structural parameters of pamidronate for the most stable conformers obtained at the B3LYP/6-311++G(d,p) level of theory in comparison with those obtained from X-ray crystallography. Bond lengths and angles are in angstroms and degrees, respectively

	Angles				Bonds		
	P_1−C_α−P_2	C−C_β−C	N−C−C_β	C−O_β	P_x−O_{xy} [a]	P_x−$O_{xy}H_{xy}$ [a]	N−C_γ
B3LYP/6-311++G(d,p) conformers							
H_3L (z1GGG$^-$G$^-$)	107.64	116.50	113.01	1.437	1.521	1.640	1.504
H_3L (z2GGTG$^-$)	112.72	120.43	113.75	1.448	1.521	1.640	1.500
H_3L (z3GGG$^-$G$^-$)	106.80	116.25	112.90	1.439	1.524	1.634	1.507
H_2L (z1GGTG$^-$)	113.44	120.84	113.28	1.451	1.541	1.639	1.497
H_2L (c2GGG$^-$G$^-$)	113.26	116.22	113.84	1.445	1.524	1.640	1.482
H_2L (c4CGTA$^+$)	111.25	118.22	111.58	1.446	1.523	1.642	1.485
H_2L (c6CGG$^-$A$^-$)	114.76	116.67	111.46	1.449	1.524	1.635	1.485
Structures from X-ray crystallography							
H_2L(z) GGG$^-$T [Ref 37]	110.25	116.55	109.02	1.452	1.515	1.613	1.492
H_3L(z) GGG$^+$T [Ref 38]	111.63	116.30	108.01	1.437	1.503	1.583	1.496

[a] Average is reported over all possible "x" and/or "y" values in a conformer

of thumb it can be said that in condensed phase any P−O bond longer than 1.6 Å is a single bond with protonated oxygen. Such a rule would be helpful for interpretation of protonation states of bisphosphonate groups in experimental structures with missing hydrogen positions.

As a result of higher bond orders the length of deprotonated P-O bonds are shorter than 1.59 Å in both gas-phase and solvated conformers. In a finer analysis, this cluster of bond lengths can be partitioned into three subsets corresponding to three types of high-order P−O bond. In the order of increasing average P−O length, these subsets correspond to equivalent bare oxygen atoms in PO_3H_2, PO_3H and PO_3 groups. In each of these subsets, the diversity and distribution of P−O bond lengths over the conformational space of pamidronate is mainly affected by different patterns of hydrogen bonding. The bare oxygen in high-order P−O bonds can only act as a hydrogen bonding acceptor which will results in elongation of P−O bond. This is reflected in Fig. 5 by the fact that all corresponding curves are skewed to the right. In this regard, hydrogen bonds between terminal amine and phosphonate groups have an especial effect that can be revealed by comparison of **c**- and **z**-form curves in Fig. 5. When the amine nitrogen becomes protonated the single P−O bonds are more shortened since the $NH_3^{(+)}$ cannot act as an acceptor for their protons. On the other hand, in zwitterionic conformers the high order P−O bonds are elongated since the $NH_3^{(+)}$ is more potent than NH_2 to act as a donor for bare oxygen atoms.

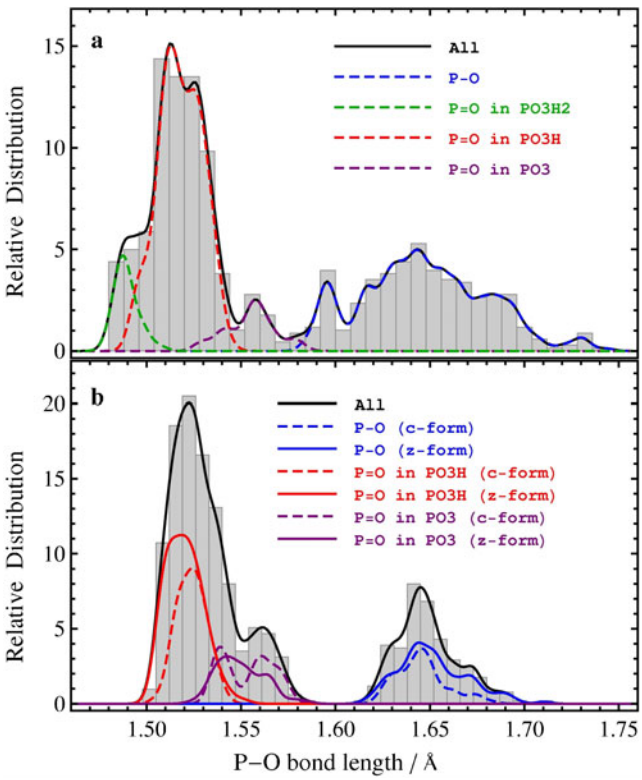

Fig. 5 Distribution of P-O bond length values over conformational space of pamidronate. **a** Gas-phase structures. **b** Solvated (C-PCM) structures

Intramolecular hydrogen bonds

In Tables 4 and S7 and S8 geometrical and topological characteristics of intramolecular hydrogen bonds in the most stable gas-phase conformers of pamidronate are listed for **H_3L**, **H_2L** and **HL** protonation states, respectively. Note that only topologically confirmed hydrogen bonds are considered in these tables. As can be seen, strongest hydrogen bonds are those occurred between phosphonate groups. In most conformations of pamidronate the alkyl amine side chain is folded on hydroxyl or phosphonate groups to participate in hydrogen bonding with them. These nitrogen containing hydrogen bonds are weaker than inter-phosphonate hydrogen bonds though they play an important role on the relative stability of conformers. A common feature of most stable conformers in all protonation states is their stronger nitrogen containing hydrogen bonds. Especially, the **c2GCTG**$^-$ conformer of **HL** in gas phase has three N−H···O contacts of which two of them belong to a bifurcated hydrogen bond between $N-H_{N2}$ and O_{11} and O_{23}. However, tendency of the amine group to participate in hydrogen bonding is reduced significantly in **HL** structures and as a result of it the sterically relaxed Trans orientation of amine becomes more populated.

Presence or absence of hydrogen bond between hydroxyl group as a donor and one of the oxygen atoms of the phosphonate groups is a somewhat mysterious feature of pamidronate conformers. In all conformers of pamidronate there is a geometrically identified hydroxyl-phosphonate hydrogen bond where the hydroxyl group is always the donor. However, many of these hydrogen bonds are not confirmed topologically. In other words, there are many cases where H_O-O_{xy} distance is less than the sum of their van der Waals radii but there is no bond critical point between them. Application of a tighter geometrical threshold is not a solution to this problem, since many topologically confirmed hydrogen bonds are not then geometrically predictable. In **H_3L** and **H_2L** protonation states both PO_3 groups prefer a staggered orientation while in the case of **HL**, the fully deprotonated phosphonate group takes an eclipsed structure. This fact is well correlated with the presence and strength of hydrogen bonds between $O_\beta-H_O$ and one of PO_3 oxygen atoms. As can be seen in Tables 4 and S7 and S8 tendency of hydroxyl group for donation of hydrogen bond to the PO_3 group is increased from **H_3L** to **HL** protonation states. Indeed most of geometrically identified $O_\beta-H_O\cdots O_{xy}$ hydrogen bonds are not topologically confirmed in **H_3L** and **H_2L** while for all of them in the

Table 4 Geometrical and topological characteristics of hydrogen bonds in the most stable conformers of H_3L protonation state. Only topologically confirmed H-bonds are listed here

Conformer	D-H···A Atom names	H···A Distance (Å)	D-H···A Angle (deg)	ρ_{bcp}	$\nabla^2_{\rho bcp}$	E_{HB} (kcal/mol)
c1GGTG$^-$	O_{11}-H_{11}···O_{23}	1.72	155.0	0.045	0.133	13.3
	O_{12}-H_{12}···O_{22}	1.97	152.8	0.026	0.080	5.9
	O_{21}-H_{21}···N	2.05	145.1	0.026	0.074	5.4
	N-H_{N1}···O_{23}	2.08	136.1	0.022	0.075	4.8
	O_β-H_O···O_{22}	2.13	126.2	0.021	0.075	5.1
	C_γ-$H_{\gamma 1}$···O_{11}	2.64	123.0	0.008	0.025	1.6
c2GGG$^-$G$^-$	O_{11}-H_{11}···O_{23}	1.77	155.2	0.039	0.119	10.8
	O_{12}-H_{12}···O_{22}	1.82	154.5	0.036	0.109	9.5
	N-H_{N2}···O_{13}	2.04	155.5	0.022	0.077	4.9
c3GGG$^-$G$^+$	O_{11}-H_{11}···O_{23}	1.77	154.6	0.035	0.120	10.9
	O_{12}-H_{12}···O_{22}	1.87	154.3	0.026	0.099	8.1
	O_β-H_O···O_{22}	2.16	125.8	0.016	0.073	4.9
	N-H_{N2}···O_{13}	2.34	136.7	0.008	0.040	2.5
	N-H_{N1}···O_β	2.58	106.9	0.007	0.035	2.0
	C_γ-$H_{\gamma 2}$···O_{13}	2.69	106.4	0.006	0.031	1.8
c4GGG$^-$G$^-$	O_{11}-H_{11}···O_{23}	1.77	155.4	0.039	0.119	10.9
	O_{12}-H_{12}···O_{22}	1.81	155.0	0.037	0.111	9.8
	N-H_{N2}···O_{13}	2.04	153.3	0.022	0.077	4.9

HL state a bond critical point was observed. Moreover, in **HL** state values of E_{HB} for O_β–H_O···O_{22} hydrogen bonds are around 5–10 kcal mol^{-1} stronger than $\mathbf{H_3L}$ or $\mathbf{H_2L}$ cases. Thus the steric strain of PO_3 eclipse orientation is compensated by stronger hydroxyl-phosphonate hydrogen bonds in **HL** protonation state.

An interesting question is how well the geometrical and topological characteristic parameters of hydrogen bonds are correlated with each other over the conformational space of pamidronate. An assessment of values reported in Tables 4 and S7 and S8 shows that the hydrogen-acceptor distance correlates better than the donor-hydrogen-acceptor angle with any of the topological parameters. In nearly all topologically confirmed hydrogen bonds and for any type of donor or acceptor atoms, one can find that shorter hydrogen-acceptor distances result in larger electron density and its Laplacian and larger local density of potential energy at hydrogen bonding critical point. In Fig. 6 the electron density at hydrogen-bond critical point is plotted against acceptor-hydrogen distance. All conformers in all protonation states are considered in this figure. Such correlations usually were performed over hydrogen bonding data of different systems and to our knowledge this is the first time that this type of correlation is tested over different conformers of a single system. In the lower panel of Fig. 6 the same data is depicted for $\ln(\rho_{bcp})$ and distinction is made between different hydrogen donors. The result of a linear regression applied to these data is also reported in this figure. As can be seen, the linear relation between $\ln(\rho_{bcp})$

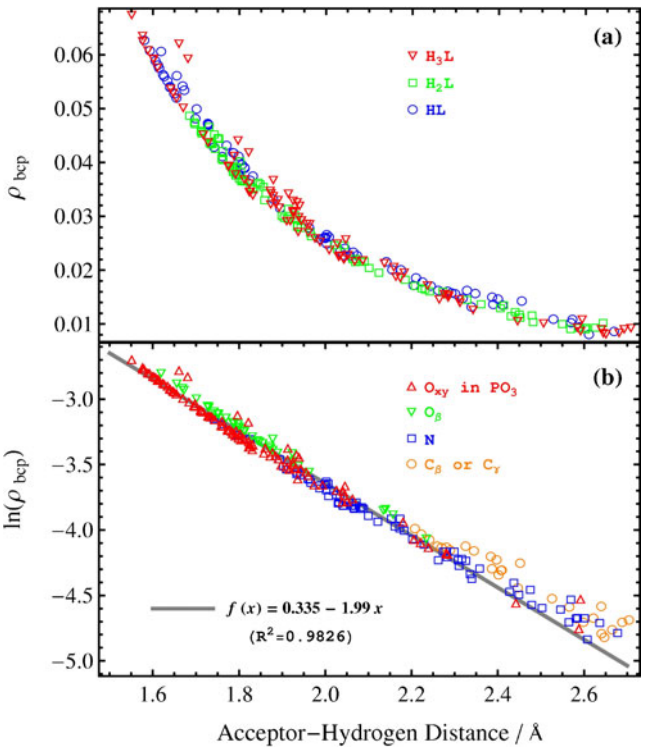

Fig. 6 **a** Correlation between electron density at H-bond critical point and the acceptor-hydrogen distance over conformational space of pamidronate. **b** The same data on a logarithmic scale with distinction between different types of donors. Electron densities larger than 0.015 were fitted with depicted linear model

and acceptor-hydrogen distance holds well for stronger hydrogen bonds. At larger acceptor-hydrogen distances the data points are more scattered. Another notable fact is that the correlation between $\ln(\rho_{bcp})$ and acceptor-hydrogen distance is independent of the protonation state of pamidronate and mainly depends on the type of donor atom. Indeed better linear regressions can be obtained if only hydrogen bonds of the same donor type are considered in the fit or if the analysis be performed on subsets of structurally similar conformers.

Conclusions

Full conformational space of pamidronate was searched for three protonation states relevant at physiological pH range. Numerous stable conformers were obtained for each state in gas phase and in the presence of continuum solvation effects. Reasonable agreement was found between bond lengths and angle values in comparison with X-ray crystal structures. Present analysis shows that in all protonation states of pamidronate only the canonical tautomer exists in the gas-phase. As a result of foldable alkyl-amine side chain one proton always migrates from $NH_3^{(+)}$ to one of the $P{-}O^{(-)}$ groups. On the other hand, the solvation effects, or strictly speaking the implicit model of solvation considered here, stabilizes the charge separation in zwitterionic forms of all $\mathbf{H_3L}$ and some $\mathbf{H_2L}$ conformers but all of the **HL** conformers remain canonical even when the solvent effects are taken into account.

The spectrum of conformational energy is populated by many low lying structures. In gas phase and within an energy range of 5 $kcal\,mol^{-1}$ higher than the most stable conformer there are 9, 15 and 8 conformers for $\mathbf{H_3L}$, $\mathbf{H_2L}$ and **HL** protonation states, respectively. Solvation effects reduces the energy differences considerably and in the same energy range 16, 14 and 18 conformers were found for $\mathbf{H_3L}$, $\mathbf{H_2L}$ and **HL** protonation states, respectively. Solvation effects also reduce the structural diversity of pamidronate as revealed from the statistical analysis of P−O bond lengths. Analysis of different contributions of molecular partition functions and conformational equilibrium constants show that the stability of conformers is mainly controlled by electronic and vibrational factors. In all conformations there is a competition between electronic and vibrational parts of equilibrium constants and as a result of it the order of stability of different conformers is changed by inclusion of thermal contributions to the Gibbs free energy.

The intramolecular hydrogen bonds were analyzed by geometrical and topological criteria. In some conformers, presence or absence of a hydrogen bond between hydroxyl and phosphonate groups remains as an open question since the geometrically identified hydrogen bonds were not confirmed by topological criteria. All other hydrogen bonds were identified as true QTAIM cases as a result of existence of a bond critical point. In all topologically confirmed hydrogen bonds there is a well behaved correlation between the geometrical parameters and those deduced from topology of electron density at hydrogen bond critical point. The best correlation was found to be a nearly linear relation between the hydrogen-acceptor distance and the logarithm of electron density at hydrogen bond critical point. Accordingly, the relative strength of different types of hydrogen bonds cover a wide range from strong phosphonate-phosphonate hydrogen bonds to the weak C−H···O or C−H···N cases.

Acknowledgments This work was supported in part by the University of Tehran Research Council. The authors would like to acknowledge financial support from the research council of Shahid Beheshti University. Also the technical support of the chemistry computational center at Shahid Beheshti University is gratefully acknowledged.

References

1. Rodan JA, Reszka AA (2002) Bisphosphonate mechanism of action. Curr Mol Med 2:571–577
2. Papapoulos SE (2008) Bisphosphonates: how do they work best. Pract Res Clin Endocrinol Metab 22:831–847
3. Coxon FP, Thompson K, Rogers MJ (2006) Recent advances in understanding the mechanism of action of bisphosphonates. Curr Opin Pharmacol 6:307–312
4. Russell RGG (2011) Bisphosphonates: the first 40 years. Bone 49:2–19
5. Rogers MJJ, Crockett JC, Coxon FP, Mönkkönen J (2011) Biochemical and molecular mechanisms of action of bisphosphonates. Bone 49:34–41
6. Montalvetti A, Bailey BN, Martin MB, Severin GW, Oldfield E, Docampo R (2001) Bisphosphonates are potent inhibitors of *Trypanosoma cruzi* Farnesyl pyrophosphate synthase. J Biol Chem 276:33930–33937
7. Ebetino FH, Roze CN et al (2005) Molecular interactions of nitrogen-containing bisphosphonates within farnesyl diphosphate synthase. J Organomet Chem 690:2679–2687
8. Gabelli SB, McLellan JS et al (2006) Structure and mechanism of the farnesyl diphosphate synthase from *Trypanosoma cruzi:* implications for drug design. Prot Struct Func Bioinform 88:62–80
9. Dunford JE, Kwaasi AA et al (2008) Structure–activity relationships among the nitrogen containing bisphosphonates in clinical use and other analogues: time-dependent inhibition of human farnesyl pyrophosphate synthase. J Med Chem 51:2187–2195
10. Kotsikorou E, Oldfield E (2003) A quantitative structure-activity relationship and pharmacophore modeling investigation of aryl-x and heterocyclic bisphosphonates as bone resorption agent. J Med Chem 46:2932–2944
11. Yin F, Cao R, Goddard A, Zhang Y, Oldfield E (2006) Enthalpy versus entropy-driven binding of bisphosphonates to farnesyl diphosphate synthase. J Am Chem Soc 128:3524–3525
12. Mukherjee S, Song Y, Oldfield E (2008) NMR Investigations of the static and dynamic structures of bisphosphonates on human bone: a molecular model. J Am Chem Soc 130:1264–1273
13. Mao J, Mukherjee S et al (2006) Solid-state NMR, crystallographic, and computational investigation of bisphosphonates and farnesyl

diphosphate synthase-bisphosphonate complexes. J Am Chem Soc 128:14485–14497
14. Mukherjee S, Huang C, Guerra F, Wang K, Oldfield E (2009) Thermodynamics of bisphosphonates binding to human bone: a two-site model. J Am Chem Soc 131:8374–8375
15. Rasanen JP, Pohjala E, Pakkanen TA (1996) *Ab initio* studies on organophosphorus compounds, part 4-intramolecular hydrogen bonding and water interactions of bisphosphonates. J Chem Soc Perkin Trans 2:39–47
16. Rasanen JP, Pohjala E, Nikander H, Pakkanen TA (1996) *Ab Initio* studies on organophosphorus compounds-5 interactions of dianionicbisphosphonate compounds with magnesium and calcium. J Phys Chem 100:8230–8239
17. Robinson J, Cukrowski I, Marques HM (2006) Modelling the interaction of several bisphosphonates with hydroxyapatite using the generalised AMBER force field. J Mol Struct 825:134–142
18. Ohno K, Mori K, Orita M, Takeuchi M (2011) Computational insights into binding of bisphosphates to farnesyl pyrophosphate synthase. Curr Med Chem 18:220–233
19. Matczak-Jon E, Videnova-Adrabinska V (2005) Supramolecular chemistry and complexation abilities of diphosphonic acids. Coord Chem Rev 249:2458–2488
20. Matczak-Jon E, Kurzak B, Kamecka A, Kafarski P (2002) Interactions of zinc(II), magnesium(II) and calcium(II) with aminomethane-1,1-diphosphonic acids in aqueous solutions. Polyhedron 21:321–332
21. Hagele G, Szakacs Z, Ollig J, Hermens S, Pfaff C (2000) NMR-controlled titrations: characterizing aminophosphonates and related structures. Heteroatom Chem 11:562–582
22. Boichenko AP, Markov VV, Kong HL, Matveeva AG, Loginov LP (2009) Re-evaluated data of dissociation constants of alendronic, pamidronic and olpadronic acids. Cent Eur J Chem 7:8–13
23. McNaught AD, Wilkinson A (1997) Compendium of chemical terminology, IUPAC, 2nd edn. Blackwell Scientific, Oxford
24. Stewart JJP (2007) Optimization of parameters for semiempirical methods V: modification of NDDO approximations and application to 70 elements. J Mol Model 13:1173–1213
25. Klamt A, Schüümann G (1993) COSMO: a new approach to dielectric screening in solvents with explicit expressions for the screening energy and its gradient. J Chem Soc Perkin Trans 2:799–805
26. Barone V, Cossi M (1998) Quantum calculation of molecular energies and energy gradients in solution by a conductor solvent model. J Phys Chem A 102:1995–2001
27. Cossi M, Rega N, Scalmani G, Barone V (2003) Energies, structures, and electronic properties of molecules in solution with the C-PCM solvation model. J Comput Chem 24:669–681
28. McQuarrie DA (1976) Statistical mechanics. HarperCollins, New York
29. Chelli R, Gervasio FL et al (2000) Conformational distribution of gas-phase glycerol. J Phys Chem A 104:11220–11222
30. Bondi A (1964) van der Waals volume and radii. J Phys Chem 68:441–451
31. Popelier P (2000) Atoms in molecules: an introduction. Prentice-Hall, Englewood Cliffs
32. Grabowski SJ (2004) Hydrogen bonding strength—measures based on geometric and topological parameters. J Phys Org Chem 17:18–31
33. Espinosa E, Molins E, Lecomte C (1998) Hydrogen bond strengths revealed by topological analyses of experimentally observed electron densities. Chem Phys Lett 285:170–173
34. MOPAC (2009) Stewart JJP, Stewart Computational Chemistry, http://OpenMOPAC.net
35. Schmidt MW, Baldridge KK et al (1993) General atomic and molecular electronic structure system. J Comput Chem 14:1347–1363
36. Biegler-König F, Schönbohm J, Bayles D (2001) AIM2000—a program to analyze and visualize atoms in molecules. J Comput Chem 22:545–559
37. Vega D, Fernandez D, Ellena JA (2002) Disodium pamidronate. Acta Crystallogr Sect C 58:m77–m80
38. Stahl K, Treppendahl SP, Preikschat H, Fischer E (2005) Sodium 3-ammonio-1-hydroxypropylidene-1,1-bisphosphonate monohydrate. Acta Crystallogr Sect E Struct Rep Online 61:m132–m134